

An advanced numerical model of elastomeric seismic isolation bearings

Manish Kumar*, Andrew S. Whittaker and Michael C. Constantinou

Department of Civil, Structural and Environmental Engineering, 212 Ketter Hall, University at Buffalo, State University of New York, Buffalo, NY 14260, U.S.A.

SUMMARY

The nuclear accident at Fukushima Daiichi in March 2011 has led the nuclear community to consider seismic isolation for new large light water and small modular reactors to withstand the effects of beyond design basis loadings, including extreme earthquakes. The United States Nuclear Regulatory Commission is sponsoring a research project that will quantify the response of low damping rubber (LDR) and lead rubber (LR) bearings under loadings associated with extreme earthquakes. Under design basis loadings, the response of an elastomeric bearing is not expected to deviate from well-established numerical models, and bearings are not expected to experience net tension. However, under extended or beyond design basis shaking, elastomer shear strains may exceed 300% in regions of high seismic hazard, bearings may experience net tension, the compression and tension stiffness will be affected by isolator lateral displacement, and the properties of the lead core in LR bearings will degrade in the short-term because of substantial energy dissipation.

New mathematical models of LDR and LR bearings are presented for the analysis of base isolated structures under design and beyond design basis shaking, explicitly considering both the effects of lateral displacement and cyclic vertical and horizontal loading. These mathematical models extend the available formulations in shear and compression. Phenomenological models are presented to describe the behavior of elastomeric isolation bearings in tension, including the cavitation and post-cavitation behavior. The elastic mechanical properties make use of the two-spring model. Strength degradation of LR bearing under cyclic shear loading due to heating of lead core is incorporated. The bilinear area reduction method is used to include variation of critical buckling load capacity with lateral displacement. The numerical models are coded in OpenSees, and the results of numerical analysis are compared with test data. The effect of different parameters on the response is investigated through a series of analyses. Copyright © 2014 John Wiley & Sons, Ltd.

Received 21 September 2013; Revised 6 March 2014; Accepted 17 March 2014

KEY WORDS: elastomeric bearing; extreme loading; cavitation; nuclear power plants; isolation

1. INTRODUCTION

The behavior of elastomeric bearings in shear and compression is well established, and mathematical models exist to reasonably capture the response expected for design basis earthquake for regular structures. These mathematical models use simplified load-deformation relationships and ignore behaviors that might be important under beyond design basis earthquakes during which elastomeric bearings may experience large strains and lateral displacement under time-varying three-dimensional loadings.

Knowledge of the tensile properties of elastomeric bearing is rather limited, and the available mathematical models do not capture the experimentally observed behavior in tension. Constantinou

*Correspondence to: Manish Kumar, Department of Civil, Structural and Environmental Engineering, 212 Ketter Hall, University at Buffalo, State University of New York, Buffalo, NY 14260, U.S.A.

†E-mail: mkumar2@buffalo.edu

et al. [1] recommended the two-spring model of Koh and Kelly [2] for vertical stiffness in compression, which has been validated experimentally by Warn *et al.* [3], and a bilinear model in tension having the same stiffness as in compression up to the point of cavitation. Yamamoto *et al.* [4] used a similar backbone curve to [1] and included hysteresis in compression and tension. This model uses the compression modulus proposed by Gent and Lindley [5] and an arbitrarily small value of post-cavitation modulus. It ignores permanent damage, reduction in cavitation strength, and effect of loading history, which might be important for beyond design basis earthquake loadings.

Dorfmann and Burtscher [6] discussed a hyperelastic model, which accounts for the reduction in bulk modulus of the rubber due to cavitation. It provides a reasonable match for the backbone curve of the load-deformation behavior of an elastomeric bearing in tension but cannot capture hysteretic behavior under cyclic loading. Dorfmann *et al.* [7] proposed a pseudo-elastic model that includes a damage parameter and four-material parameters to capture permanent damage due to cyclic tensile loading, wherein a dilatational strain energy function must be assumed to relate hydrostatic pressure to the volume change in the rubber. These formulations are more amenable to finite element analysis of a single bearing.

In addition to the models discussed above, other researchers have proposed empirical formulae for stiffness and cavitation strength [8, 9]. However, these formulae are based on limited experimental results, and a robust mathematical formulation for use in structural analysis cannot be obtained from these models. A new phenomenological model that can capture tensile response of seismic isolation elastomeric bearings observed from experiments is presented, and the effect of tensile properties on the response is discussed. The total number of parameters required for the application of the proposed model is minimized, and recommendations are provided for the values of parameters on the basis of available experimental data and sensitivity analyses.

The mechanical properties of an elastomeric bearing in all degrees of freedom are integrated using a physical model. Yamamoto *et al.* [4] and Kikuchi *et al.* [10] presented physical models of circular and square bearings, which use complex arrangements of shear and axial springs to simulate stability and shear effects under varying vertical load. The conventional two-node link element is used here owing to its efficiency and ease of implementation for seismic response analysis of nuclear power plants, base isolated using hundreds of such bearings.

2. MOTIVATION

Earthquake hazards used for the analysis, design, and assessment of safety-related nuclear structures are defined using return periods of between 10,000 and 100,000 years. Such return periods are much longer than those used for the analysis and design of buildings and bridges for which return periods range between 500 and 2500 years. Although traditional models of seismic bearings are suitable for predicting the response of seismically isolated buildings and bridges, their applicability and usefulness is unknown for the extreme ground motions considered for nuclear structures. The forthcoming seismic isolation NUREG [11] and Section 7.7 of ASCE 4 [12] require that isolators be *analyzable* across the range of responses expected in design basis shaking and beyond design basis shaking, which may include, for elastomeric bearings, the following considerations:

- (1) Coupled bidirectional motion in horizontal directions
- (2) Coupling of vertical and horizontal motion
- (3) Cavitation and post-cavitation behavior in tension
- (4) Strength degradation in cyclic tensile loading due to cavitation
- (5) Variation in critical buckling load capacity due to lateral displacement
- (6) Strength degradation in cyclic shear loading due to heating of lead core

An integrated numerical model capable of addressing these six issues does not exist and is proposed herein, substantially expanding existing capabilities to address extreme earthquake loadings. The model is verified and validated following ASME best practices [13] and implemented in OpenSees [14] to enable use by researchers and the design professional community.

3. PHYSICAL MODEL

The physical model of an elastomeric bearing is considered as a two-node, 12 degrees-of-freedom discrete element. The two nodes are connected by six springs that represent the mechanical behavior in the six basic directions of a bearing. The degrees of freedom and discrete spring representation of an elastomeric bearing is shown in Figure 1.

The general form of element force vector, \mathbf{f}_b , and element stiffness matrix, \mathbf{K}_b , for element representation considered above is given by Eqn (1).

$$\mathbf{f}_b = \begin{bmatrix} \text{Axial} \\ \text{Shear1} \\ \text{Shear2} \\ \text{Torsion} \\ \text{Rotation1} \\ \text{Rotation2} \end{bmatrix}; \quad \mathbf{K}_b = \begin{bmatrix} \text{Axial} & 0 & 0 & 0 & 0 & 0 \\ 0 & \text{Shear1} & \text{Shear12} & 0 & 0 & 0 \\ 0 & \text{Shear21} & \text{Shear2} & 0 & 0 & 0 \\ 0 & 0 & 0 & \text{Torsion} & 0 & 0 \\ 0 & 0 & 0 & 0 & \text{Rotation1} & 0 \\ 0 & 0 & 0 & 0 & 0 & \text{Rotation2} \end{bmatrix} \quad (1)$$

The coupling of the two shear springs is considered directly by using a coupled bidirectional model. All other springs are uncoupled. The coupling of vertical and horizontal directions are considered indirectly by using expressions for mechanical properties in one direction that are dependent on the response parameters in the other direction. Linear uncoupled springs are considered in the torsion and the two rotational springs as they are not expected to significantly affect the response of an elastomeric bearing. The off-diagonal terms due to coupling between axial and shear, and axial and rotation, are not considered in the two-spring model [2] used here. An exact model would have nonzero values of these off-diagonal terms. A discussion on the formulation of the two-spring model and the exact model is presented in [15]. The subscript b refers to the element's basic coordinate system. When the model is implemented in software programs, response quantities are transformed between the basic, local, and global coordinates to perform computations.

The discrete spring model presented here has the advantages of easy implementation and being computationally efficient. The structural analysis software programs that allow user to add functionalities through user created elements (e.g., OpenSees and ABAQUS) provide a framework for such implementation. The mechanical properties of the six springs (also referred to as material models in OpenSees) are defined using analytical solutions available from the analysis of elastomeric bearings. These material models are discussed in the following sections. The expression for mechanical

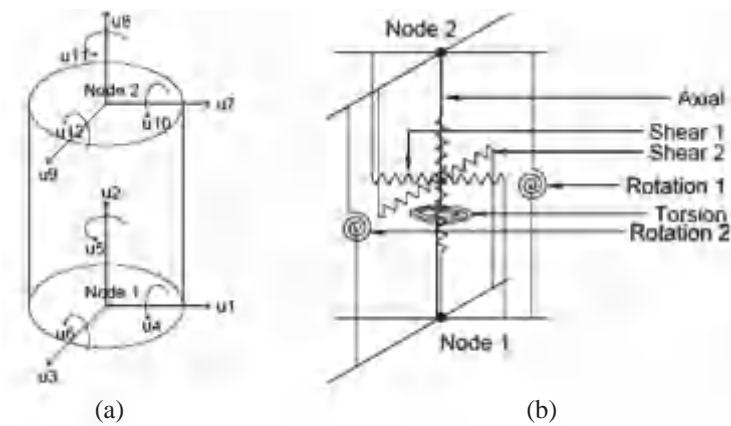


Figure 1. Physical model of an elastomeric bearing. (a) Degrees of freedom and (b) discrete spring model representation.

properties, including stiffness and buckling load capacity, are derived using explicit consideration for geometric nonlinearity due to large displacement effects. The $P - \Delta$ effect, which is an approximate method to account for geometric nonlinearity in structural analysis problems, is therefore not considered. The physical model and the mechanical properties of elastomeric bearings in horizontal and vertical direction are discussed here for low damping rubber (LDR) bearing and lead rubber (LR) bearing. The authors have extended the model for high damping rubber (HDR) bearings using an appropriate mathematical model for the horizontal shearing behavior, but that model is not discussed here.

4. BEHAVIOR UNDER AXIAL LOADING

4.1. Behavior in tension

Only elastomeric bearings that provide horizontal isolation are considered appropriate at this time for nuclear applications, although there have been recent efforts to isolate in the horizontal and vertical directions (e.g., Vu *et al.* [16]). Tensile deformation in elastomeric bearings has traditionally been considered undesirable. Design codes and standards that explicitly acknowledge response in axial tension either do not allow tensile loading or limit the value of allowable tensile stress in elastomeric bearings under design-basis loading. The Japanese specifications for design of highway bridges [17] limit the tensile stress in G8 and G10 rubber (rubber classes with shear modulus 0.8 and 1 MPa) to 2 MPa. Eurocode 8 restricts the use of elastomeric bearings if axial tensile force is expected during seismic loadings [18]. The Chinese seismic design code limits the tensile stress to 1 MPa [19].

Experiments have shown that elastomeric bearings can sustain large tensile strains up to 100%, following cavitation, without rupture [9]. The design codes and guidelines for seismic isolation of nuclear power plants in the USA [11, 12] consider the effects of beyond design basis earthquake loadings, which may produce net tensile force in one or more bearings. Similarly, the use of isolation for tall buildings may result in tensile loading for design basis and beyond design basis shaking. In order to consider tensile loading in seismic isolator design, the tensile properties of elastomeric bearings need to be investigated, and robust mathematical models are required to simulate the load-deformation behavior in tension.

4.2. Experimental investigation of behavior in tension

Much of the initial work on cavitation of elastomers was carried out by Gent and Lindley [20]. They used bonded rubber cylinders in their experiments to investigate the behavior under tensile loading. The tensile properties of rubber are highly dependent on thickness, or more appropriately the shape factor, S , which is defined as the bonded rubber area of an elastomeric bearing divided by the perimeter area that is free to bulge. Experimental data on the elastomeric bearings with high shape factors (between 5 and 30) that are used for seismic isolation applications is limited. A summary of the experimental work on the tensile properties of elastomeric bearing is presented in Table I.

Table I. Experimental work on the tensile properties of elastomeric bearings.

Reference	Bearing properties	Focus
Clark [21]	HDR, diameter 176 mm, shape factor ~20	Monotonic tensile failure
Iwabe <i>et al.</i> [9]	LDR, LR, HDR bearings, diameter 500 and 1000 mm, shape factor ~30	Tension, shear-tension, post-tension mechanical properties
Takayama <i>et al.</i> [22]	LDR, diameter 500 and 1000 mm, varying bearing plate thickness, shape factor ~33	Tension, scale effect, bearing plate thickness
Shoji <i>et al.</i> [23]	LR, 240 × 240 mm, shape factor ~8	Cyclic deterioration under tension
Feng <i>et al.</i> [24]	LR, diameter 100 mm, shape factor ~15	Tension, mechanical properties, three-dimensional dynamic loading
Warn [25]	LDR, LR, outer diameter 152 mm, inner diameter 30 mm, shape factor ~12	Tension, coupling of horizontal and vertical motion
Constantinou <i>et al.</i> [1]	LDR, diameter 250 mm, shape factor ~9	Single cycle tensile loading

Figures 2 and 3 present the behavior of LDR bearings obtained under pure tension and tension with shear, respectively.

Some of the important conclusions of these experimental studies are as follows:

- (1) Substantial reduction of tensile stiffness occurs at a critical tensile stress (cavitation stress) that depends on the shear modulus and shape factor.
- (2) Load-deformation behavior in tension is linear up to cavitation with the tensile stiffness approximately equal to the compression stiffness, followed by nonlinear post-cavitation behavior.
- (3) Tension coupled with shear loading increases the tensile load and deformation capacity of a bearing when compared with pure tension.
- (4) Cavitation has no major effect on the compression and shear characteristics of a bearing.
- (5) Under cyclic loading the tensile strength decreases, and the extent of reduction is a function of maximum tensile strain experienced in previous cycles.
- (6) State of tension during shear loading has minimal effect on shear stiffness and shear hysteresis loops.

4.3. Cavitation

An elastomeric bearing under tensile loading is characterized by the formation of cavities in the volume of rubber. Gent and Lindley [20] explained that the fracture inside a rubber layer occurs at a critical hydrostatic stress value that is related to a critical value of applied tensile stress. This critical tensile stress is equal to the hydrostatic stress for large shape factor bearings where critical hydrostatic stress is attained uniformly over most of the bonded area, except at boundaries. This is in contrast to low shape factor bearings where critical hydrostatic stress is attained only in the central area and

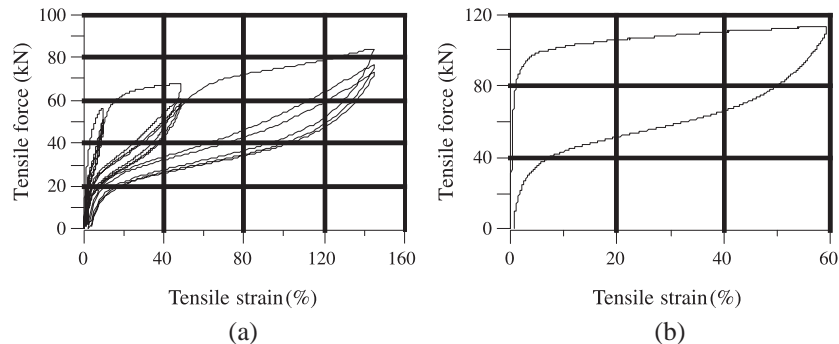


Figure 2. Load-deformation behavior of LDR bearing under cyclic tension. (a) Warn [25] and (b) Constantinou *et al.* [1].

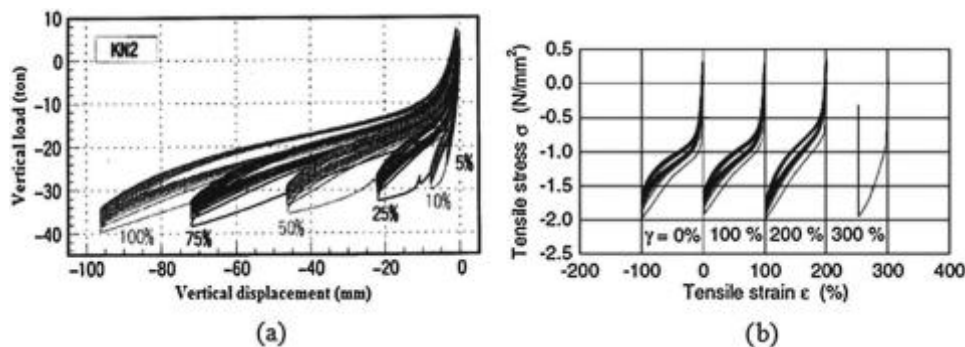


Figure 3. Load-deformation behavior of LDR bearings in cyclic tension with lateral offset. (a) 200% lateral offset [9] and (b) varying lateral offset [22].

value of the critical tensile stress is about half of the critical hydrostatic stress. This critical stress, known as cavitation stress, depends mainly on the rubber compound.

Cavitation is followed by the substantial reduction of the vertical stiffness indicated by highly discernible transition on the tensile load-deformation curve. The transition becomes smoother as the shape factor decreases, and it is generally difficult to locate the cavitation point on the load-deformation curve for bearings with shape factor less than 10. Gent [26] suggested that cavitation occurs at a negative pressure of about $3G$. The shear modulus, G , is obtained experimentally from testing at a moderate shear strains under nominal axial loads, in which the shear modulus G is relatively constant with respect to increasing shear strain, as explained in a later section. The cavitation force is

$$F_c = 3GA_0 \quad (2)$$

where A_0 is the bonded rubber area before cavitation in the rubber. For LR bearings, the lead core is neglected in performing the cavitation calculations.

It is usually difficult to estimate the strain at which cavitation occurs, because cavitation itself is difficult to locate precisely on the load-deformation curve. The pre-cavitation tensile stiffness, which is assumed to be constant for analysis purposes, decreases with axial strain even before cavitation. Although the assumption of constant pre-cavitation stiffness is appropriate for most response calculations, the cavitation strain obtained using cavitation force and pre-cavitation tensile stiffness does not reflect experimental observations. Experiments suggest that sharp change in tensile stiffness occur at a strain in the range of 2% to 5%. The cavitation strain also depends on shape factor and rubber compound. Cavitation displacements between 3 and 4 mm have been observed from experiments [1, 9, 25].

4.4. Post-cavitation behavior

The nonlinear characteristics of natural rubber are influenced by volume of fillers and the cross-linking of the polymer chains in the elastomer [27]. The reduction in stiffness after cavitation is due to breakage of rubber-filler bonds. The subsequent increase in stiffness at large strains is due to limited extensibility of polymer chains and strain crystallization [6].

Most of the available mathematical models use a very small value of post-cavitation stiffness of an arbitrary magnitude. Constantinou *et al.* [1] proposed a post-cavitation stiffness as follows:

$$K_{\text{post-cavitation}} = \frac{EA}{T_r} \quad (3)$$

where E is the elastic modulus of rubber. This formulation is proposed because following the formation of cracks after cavitation, rubber loses its triaxial state of stress and experiences uniaxial tensile stress, and the elastic modulus used in Eqn (3) is the Young's modulus of rubber.

Experiments have shown that the post-cavitation stiffness of elastomeric bearings decreases with increasing tensile deformation. It is assumed here that area used in Eqn (3) is the "true area" of the bearing excluding the total area of cavities that change with tensile deformation. The true area of bearing is equal to the bonded rubber area at the onset of cavitation and decreases as the number and size of cavities increase with tensile deformation. The reduction in true area can be attributed to two factors: (1) number of cavities and (2) size of cavities. For low shape factor bearings, there is a stress concentration toward the center, and the critical stress is attained first in the central area of the bearing. The reduction in the area of low shape factor bearings is mainly due to the increase in the size of cavities. For high shape factor bearings used in seismic isolation applications, the critical stress is obtained uniformly over the bonded rubber area, and the reduction in area is due to an increase in the number of cavities. If the rubber area is considered to be made up of infinite number of small area elements, every time a cavity is formed, an area element is eroded. The greater the area, the greater the rate of erosion of area elements. So the rate of reduction of true area with respect to tensile deformation is proportional to the instantaneous true area. Mathematically, the above hypothesis can be expressed as follows:

$$\frac{A}{u} = -kA \quad (4)$$

where k is a proportionality constant defined as the cavitation parameter, which is constant for a particular elastomeric bearing and describes the post-cavitation variation of tensile stiffness. The true area of the bearing is equal to the bonded rubber area A_0 at onset of cavitation ($u = u_c$) and decreases with tensile deformation. Integrating Eqn (4), the variation of area with tensile deformation is obtained as follows:

$$A = A_0 e^{-k(u-u_c)} \quad (5)$$

The instantaneous post-cavitation stiffness of bearing is given by

$$K_{\text{post-cavitation}} = \frac{EA}{T_r} = \frac{EA_0}{T_r} e^{-k(u-u_c)} \quad (6)$$

If $K_0 = EA_0/T_r$ is the initial post-cavitation stiffness just after the cavitation, which assumes that an infinite number of infinitely small cavities form instantaneously so that the modulus becomes Young's modulus, E , and the area still remains, A_0 , the above equation can also be rewritten as follows:

$$K_{\text{post-cavitation}} = K_0 e^{-k(u-u_c)} \quad (7)$$

Equation (7) describes the post-cavitation variation of tensile stiffness of an elastomeric bearing. It decreases exponentially, and the rate of decrease is controlled by the parameter k . To obtain the tensile load variation with tensile displacement, post-cavitation stiffness is written as $K_{\text{post-cavitation}} = F/u$, where F is the tensile force in the bearing. Equation (7) can be rewritten as follows:

$$\frac{F}{u} = \frac{EA}{T_r} = \frac{EA_0}{T_r} e^{-k(u-u_c)} \quad (8)$$

Noting that $E \approx 3G$ for rubber and the cavitation strength $F_c \approx 3GA_0$, Eqn (8) can be integrated from (F_c, u_c) to (F, u) , to obtain the tensile force in a bearing as follows:

$$F = F_c \left[1 + \frac{1}{kT_r} \left(1 - e^{-k(u-u_c)} \right) \right] \quad (9)$$

The relationship in Eqn (9) can also be formulated in terms of stress, σ , and strain, ϵ . Using the expression $F = A\sigma$, Eqn (8) can be rewritten as follows:

$$A \frac{\sigma}{u} + \frac{A}{u} = \frac{EA_0}{T_r} e^{-k(u-u_c)}$$

Substituting $A/u = -kA$ and $u = T_r$, the above equation is simplified to

$$\sigma = E + kT_r \quad (10)$$

where E/kT_r is the post-cavitation modulus, E_{post} , of elastomeric bearing. Note that there is an additional stress-dependent term (kT_r) in the post-cavitation modulus. Solving the above differential equation, the expression for post-cavitation stress is obtained as follows:

$$= c \left[e^{kT_r(u - c)} + \frac{1}{kT_r} (e^{kT_r(u - c)} - 1) \right] \quad (11)$$

where $c = 3G$ is the cavitation stress in the bearing. The same expression for stress is obtained if post-cavitation tensile force, F , in Eqn (9) is divided by the corresponding area, A , in Eqn (5).

The variation of tensile force with tensile deformation is shown in Figure 4. The parameter k for a particular bearing depends on the rubber compound and construction quality of the bearing. It is obtained by calibration with experimental data. As k increases, the rate of change of post-cavitation stiffness decreases. The value of $k=0$ corresponds to the bilinear stiffness model discussed in Constantinou *et al.* [1], and for a very large value of k , a bilinear curve with zero post-cavitation stiffness is obtained. The proposed model does not capture the minor stiffening effects that are observed during tensile loading of an elastomeric bearing at large tensile strains ($> 100\%$) because of limited extensibility of the polymer chains in rubber, but tensile strains of this order are not anticipated, even under beyond design basis loadings.

4.5. Strength degradation under cyclic loading

Cavitation in an elastomeric bearing is accompanied by irreversible damage due to the formation of microcracks in the volume of rubber. When a bearing is loaded beyond the point of cavitation and unloaded, it returns along a new path, and the cavitation strength is reduced. The area enclosed between loading and unloading amounts to the hysteretic energy due to damage in the bearing. Subsequent loading follows the latest unloading path elastically until strain exceeds the past maximum value u_{max} , below which loading has the effect of only opening and closing of existing cavities within the rubber. Once loading exceeds the past maximum value of tensile strain, the formation of new cavities leads to increased damage and follows the post cavitation behavior defined previously by Eqn (9). Upon load reversal, it again traces back a new unloading path, and the cavitation strength is further reduced. Unloading paths can be approximated by straight lines between the point of maximum strain (F_{max}, u_{max}) and the point of reduced cavitation strength (F_{cn}, u_{cn}). (F_{max}, u_{max}) and (F_{cn}, u_{cn}) change with increasing number of cycles. To capture this behavior mathematically, a damage index α is defined such that the updated cavitation strength as a function of initial cavitation strength is given by the expression:

$$F_{cn} = F_c (1 - \alpha) \quad (12)$$

The damage index α represents the cumulative damage in the bearing ($0 \leq \alpha \leq 1$). It is a function of maximum deformation experienced by the bearing under tensile loading. Mathematically, it can be expressed as $\alpha = f(u_{max})$, where f satisfies the following relations: (1) $f(u_c) = 0$ (no strength reduction up to cavitation deformation) and (2) $f(u_{max}) \rightarrow 1$ (α_{max} damage index converges to a maximum value

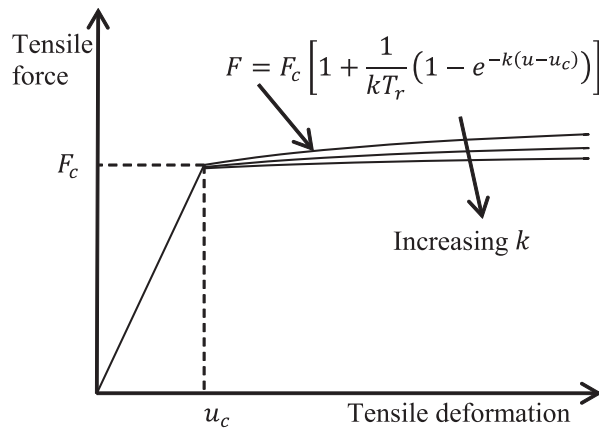


Figure 4. Post-cavitation behavior.

after large deformations). It implies that function f would be a nonlinear and monotonically increasing function that is continuous in its domain. Moreover, the damage index converges to a maximum value \max , requiring f to be an asymptotic function. A function satisfying these properties is given by

$$= \max \left[1 - e^{-a\left(\frac{u-u_c}{u_c}\right)} \right] \quad (13)$$

where parameter a is a strength degradation parameter that defines the rate of damage and \max is the maximum damage that can be expected in a bearing. The load-deformation behavior of elastomeric bearings under cyclic tensile loading is summarized in Figure 5.

4.6. Coupling of horizontal and vertical motion

The coupling of horizontal and vertical behavior is considered by (1) variation of shear stiffness with axial load and (2) dependence of axial stiffness on lateral displacement.

Two models are used for the elastic analysis of elastomeric bearings under axial loading. The continuous beam model [28, 29] is an extension of the work of Haringx [30]. The two-spring model [2], presented in Figure 6, is a simplification of the continuous beam model.

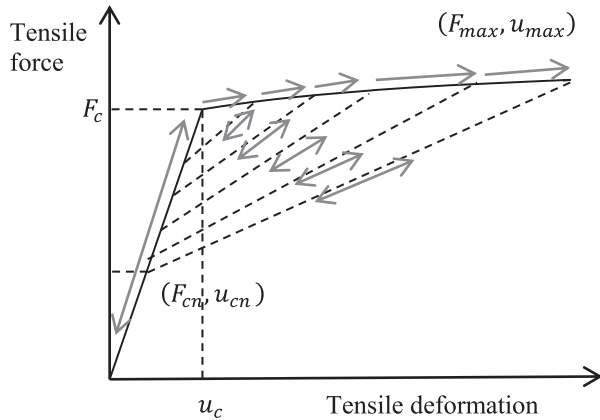


Figure 5. Strength reduction under cyclic loading.

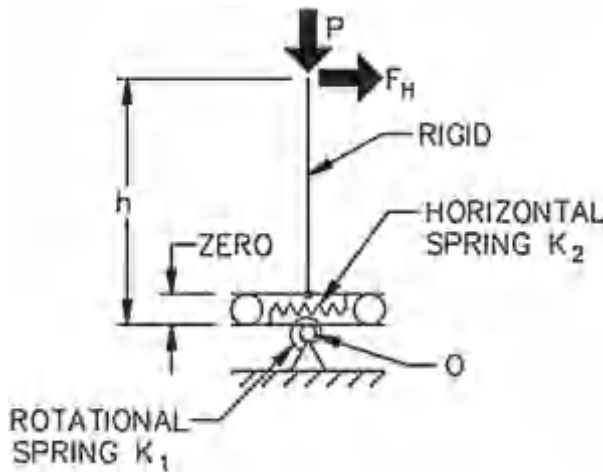


Figure 6. Model of an elastomeric bearing [1].

The two-spring model provides results that are close to the continuous beam model and is used here to obtain expressions for mechanical properties of elastomeric bearings. The two-spring model has been validated experimentally by Warn *et al.* [3] and used here owing to its robust formulation and ease of numerical implementation. The vertical stiffness of the elastomeric bearing obtained from the two-spring model is given as follows:

$$K_v = \frac{AE_c}{T_r} \frac{1}{\left[1 + \frac{3}{\pi^2} \left(\frac{u_h}{r}\right)^2\right]} \quad (14)$$

where A is the bonded rubber area, E_c is the compression modulus of the bearing calculated as average axial stress divided by the average axial strain in a rubber layer, T_r is the total rubber thickness, u_h is the lateral displacement of the bearing, and r is the radius of gyration of the bonded rubber area. The axial load-deformation curve in compression is shown in Figure 7. P_{cr} is the instantaneous value of critical buckling load, as discussed in the following section.

The effect of axial load on the horizontal stiffness of an elastomeric bearing becomes important only when the axial load is close to the critical buckling load capacity of the bearing. Koh and Kelly [2] provide an analytical expression for the horizontal stiffness as a function of the axial load using two-spring model. An approximation of the analytical expression for the horizontal stiffness that provides very accurate result is given as follows [29]:

$$K_H = \frac{GA}{T_r} \left[1 - \left(\frac{P}{P_{cr}}\right)^2\right] = K_{H0} \left[1 - \left(\frac{P}{P_{cr}}\right)^2\right] \quad (15)$$

where K_{H0} is the horizontal stiffness at zero axial load.

4.7. Buckling in compression

Han *et al.* [31] presents the capability of the available analytical models to predict the critical loads and displacements in elastomeric bearings at large shear deformations. The critical buckling load, P_{cr} , in compression is given by the expression derived in the two-spring model. The load, P_{cr} , decreases with increasing lateral displacement. The area-reduction method considers the dependence of P_{cr} on lateral displacement and provides conservative results [32]. The reduced critical buckling load is given by $P_{cr} = P_{cr} A_r / A$, where A_r is the reduced area of a bearing of diameter D due to lateral displacement u_h . For circular bearings of bonded area of diameter D , reduced area is given as $A_r = (D^2/4)(1 - \sin \theta)$, where $\theta = 2 \cos^{-1}(u_h/D)$ is the angle subtended by the chord of the overlap area at the center of the bearing. The area-reduction method suggests zero capacity for a bearing at a horizontal displacement equal to the diameter of the bearing. However, experiments have shown that a bearing does not lose all its capacity but maintains a minimum capacity after the overlapping area

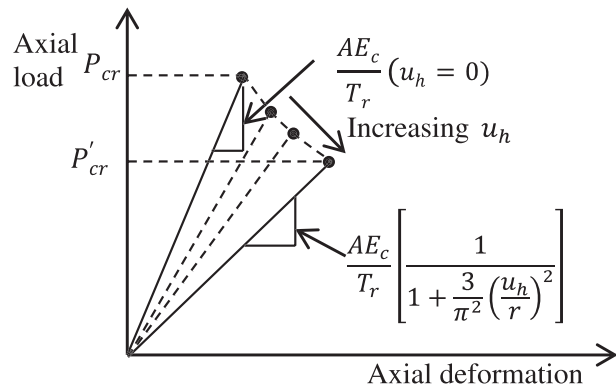


Figure 7. Stress softening under compression.

reduces to zero [3, 33, 34]. The model suggested by Warn *et al.* [3] is considered here, which uses a bilinear approximation of the area-reduction method and takes into account the finite buckling capacity of a bearing at zero overlap area. The reduced critical load is given by

$$P_{cr} = \begin{cases} P_{cr} \frac{A_r}{A} & \text{for } \frac{A_r}{A} \geq 0.2 \\ 0.2P_{cr} & \frac{A_r}{A} < 0.2 \end{cases} \quad (16)$$

The bilinear approximation of the area-reduction model is illustrated in Figure 8. The contribution of the lead core, if any, is neglected in the calculation of the critical buckling load.

4.8. Mathematical model in axial direction

A mathematical model of an elastomeric bearing in the axial direction is presented in Figure 9, which captures the following characteristics in the axial direction: (1) buckling in compression, (2) coupling of vertical and horizontal motions, (3) cavitation, (4) post-cavitation behavior, and (5) strength degradation due to cyclic loading. The model uses three unknown parameters: (1) a cavitation parameter, k , (2) a strength degradation parameter, a , and (3) a damage index, ϕ_{max} .

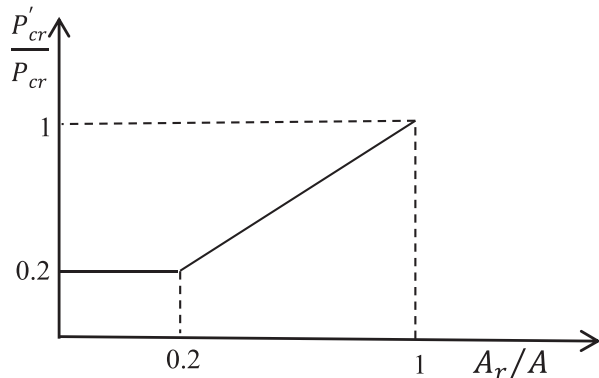


Figure 8. Bilinear variation of buckling load.

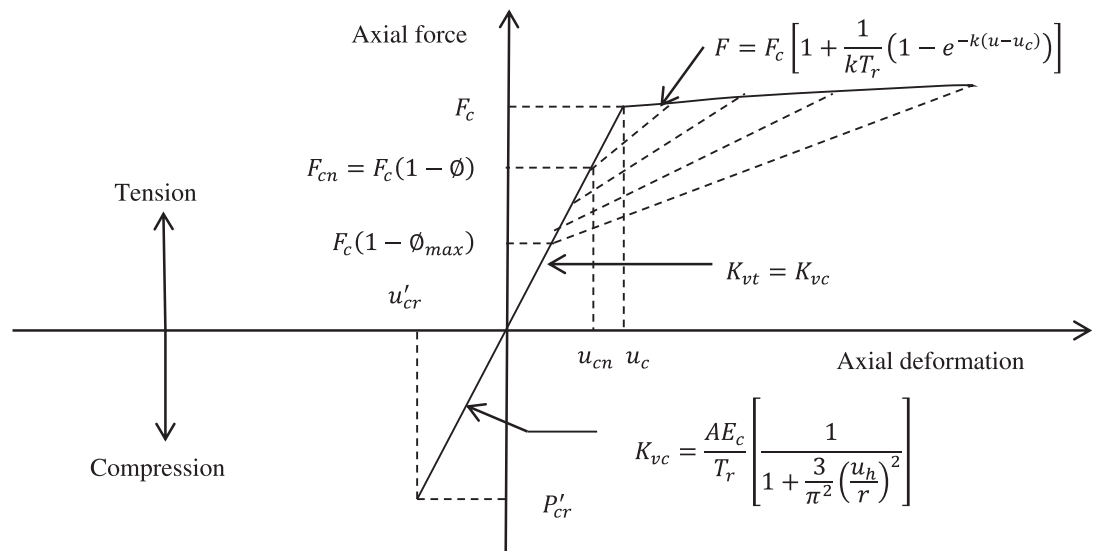


Figure 9. Mathematical model of elastomeric bearings in axial direction.

5. BEHAVIOR UNDER SHEAR LOADING

5.1. Coupled bidirectional model

A smooth bidirectional hysteretic model, shown in Figure 10, is often used for elastomeric bearings in horizontal shear. It is based on the Bouc–Wen model [35, 36] and extended for analysis of seismic isolators under bidirectional motion [37].

Parameters have been expressed here in the form that is typical of seismic isolation design, namely initial elastic stiffness, K_{el} , characteristic strength, Q_d , yield strength, F_Y , yield displacement, Y , and post-elastic stiffness, K_d . The isotropic formulation of the model in terms of restoring forces in orthogonal directions, F_x and F_y , is given by the following equation [37, 38]:

$$\begin{Bmatrix} F_x \\ F_y \end{Bmatrix} = c_d \begin{Bmatrix} \dot{U}_x \\ \dot{U}_y \end{Bmatrix} + K_d \begin{Bmatrix} U_x \\ U_y \end{Bmatrix} + (\gamma_L A_L) \begin{Bmatrix} Z_x \\ Z_y \end{Bmatrix} \quad (17)$$

where γ_L is the effective yield stress of lead, A_L is the cross-sectional area of lead-core, and c_d is a parameter that accounts for the viscous energy dissipation in rubber. The variables Z_x and Z_y represents the hysteretic component of the restoring forces. Both have units of displacement and are function of the histories of U_x and U_y . The biaxial interaction is given by the following differential equation (e.g., [36], [39]):

$$Y \begin{Bmatrix} \dot{Z}_x \\ \dot{Z}_y \end{Bmatrix} = \left(A[I] - \begin{bmatrix} Z_x^2 (\text{Sign}(\dot{U}_x Z_x) +) & Z_x Z_y (\text{Sign}(\dot{U}_y Z_y) +) \\ Z_x Z_y (\text{Sign}(\dot{U}_x Z_x) +) & Z_y^2 (\text{Sign}(\dot{U}_y Z_y) +) \end{bmatrix} \right) \begin{Bmatrix} \dot{U}_x \\ \dot{U}_y \end{Bmatrix} \quad (18)$$

Parameters and control the shape of the hysteresis loop, and A is the amplitude of the restoring force. When yielding commences, the solution of Eqn (18) is given by the equations $Z_x = \cos \theta$, $Z_y = \sin \theta$, provided the parameters satisfy the relationship $A/(+) = 1$ [40], where represents the direction of the resultant force with respect to the direction of motion and is given by expression $\theta = \tan^{-1}(\dot{U}_y/\dot{U}_x)$. The interaction curve given by this expression is circular and Z_x and Z_y are bounded by the values of ± 1 .

The first two terms on the right side of Eqn (17) represents the contribution by rubber and the third term represents the contribution by lead core to the total resisting force in the elastomeric bearing. It should be noted that the yield strength of LR bearings is contributed by the lead core; however, in LDR bearing, it is estimated on the basis of the equivalent damping assumed for the analysis, because information on damping provided by the rubber compound is not always available. This is discussed further in a later section.

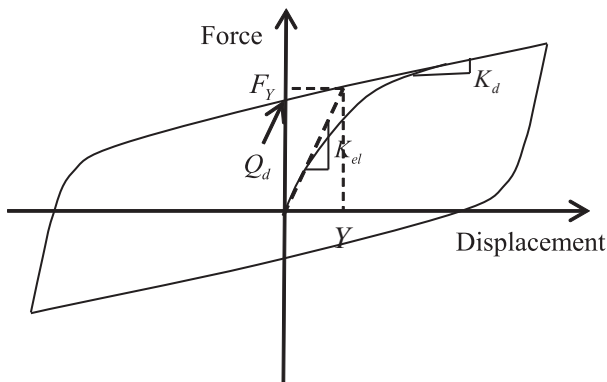


Figure 10. Mathematical model in shear.

5.2. Heating in the lead core

For LR bearings, the effective yield stress of lead used in Eqn (17) is not constant but decreases with number of cycles because of the heating of the lead-core under large cyclic displacements. The extent of reduction depends on the geometric properties of bearing and speed of motion. Kalpakidis *et al.* [41] proposed the dependence of characteristic strength of LR bearings on the increase in the temperature of lead-core, T_L , which itself is a function of time. The set of equations describing heating of the lead-core is as follows:

$$\dot{T}_L = \frac{\gamma_L(T_L)\sqrt{Z_x^2 + Z_y^2}\sqrt{\dot{U}_x^2 + \dot{U}_y^2}}{c_L h_L} - \frac{k_s T_L}{a c_L h_L} \left(\frac{1}{F} + 1.274 \left(\frac{t_s}{a} \right) ()^{-1/3} \right) \quad (19)$$

$$F = \begin{cases} 2\left(\frac{\pi}{\alpha}\right)^{1/2} - \left(\frac{\pi}{\alpha}\right) \left[2 - \left(\frac{1}{4}\right) - \left(\frac{1}{4}\right)^2 - \frac{15}{4} \left(\frac{1}{4}\right)^3 \right]; & \alpha < 0.6 \\ \frac{8}{3\pi} - \frac{1}{2(\pi\alpha)^{1/2}} \left[1 - \frac{1}{3(4\alpha)} + \frac{1}{6(4\alpha)^2} - \frac{1}{12(4\alpha)^3} \right]; & \alpha \geq 0.6 \end{cases} \quad (20)$$

$$= \frac{s t}{a^2} \quad (21)$$

$$\gamma_L(T_L) = \gamma_{L0} e^{-E_2 T_L} \quad (22)$$

The geometrical parameters h_L , t_s , and a are described in Figure 11; h_L is the height of lead-core, a is the radius of the lead core, t_s is the total thickness of the shim plates in the bearing, c_L is the specific heat of lead, ρ_L is the density of lead, s is the thermal diffusivity of steel, k_s is the thermal conductivity of steel, γ_{L0} is the effective yield stress of lead at the reference temperature, α is a dimensionless time parameter, and t is the time since the beginning of motion. Eqn (22) predicts the characteristic strength of an LR bearing as a function of instantaneous temperature obtained from Eqn (19) through parameter E_2 .

Typical values of parameters related to lead and steel from Kalpakidis *et al.* [41] are listed in Table II.

5.3. Equivalent damping

The damping in LR bearings is primarily contributed by the energy dissipation in the lead-core; the contribution of viscous damping in the rubber is typically neglected. The force-displacement loop of an elastomeric bearing is idealized per Figure 12. The effective period, stiffness, and damping of the isolated system are calculated using the following equations [42, 43]:

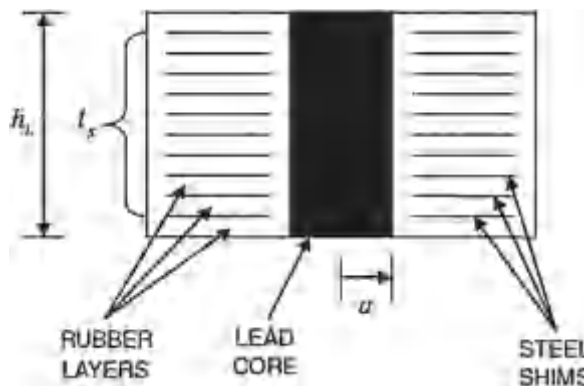
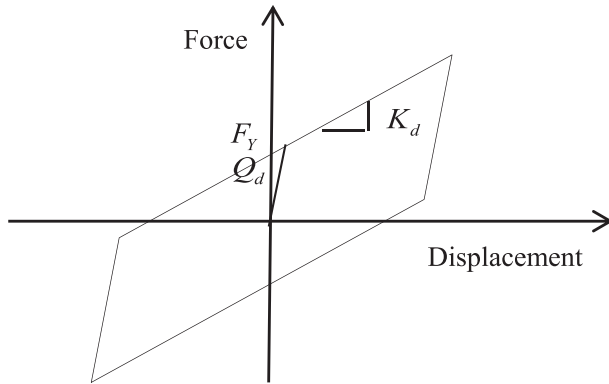


Figure 11. Schematic of an LR bearing [41].

Table II. Typical value of lead and steel related parameters.

Parameter	Value
ρ_L	11200 kg/m ³
c_L	130 J/(kg °C)
k_s	50 W/(m °C)
E_2^s	1.4×10^{-5} m ² /s
E_2	0.0069/°C

**Figure 12.** Idealized behavior in shear.

$$T_{\text{eff}} = 2\pi \sqrt{\frac{W}{K_{\text{eff}} g}} \quad K_{\text{eff}} = K_d + \frac{Q_d}{D} \quad \zeta_{\text{eff}} = \frac{1}{2\pi} \left[\frac{EDC}{K_{\text{eff}} D^2} \right] \quad (23)$$

where D is the horizontal displacement of the system due to earthquake shaking obtained from smoothed response spectra, and EDC is the energy dissipated per cycle at displacement D . For the idealized behavior shown in Figure 12, E is given as $E = 4Q_d(D - Y)$, where Y is the yield displacement of the system. The characteristic strength of an LR bearing is determined using the effective yield stress of lead core. However, for LDR bearings, the characteristic strength cannot be obtained directly. An effective damping, ζ_{eff} , of system is assumed, and characteristic strength is determined as follows:

$$\zeta_{\text{eff}} = \frac{1}{2\pi} \left[\frac{4Q_d(D - Y)}{K_{\text{eff}} D^2} \right] \leq \frac{2Q_d}{\pi K_d D} \quad (24)$$

$$Q_d \geq \frac{\pi}{2} \times \zeta_{\text{eff}} \times K_d \times D \quad (25)$$

The characteristic strength of LDR bearings can be estimated if the value of displacement D due to earthquake shaking is known from the simplified analysis [44]. If the analysis for the estimation of damping in isolated system is not performed, a nominal damping between 2% and 4% can be assumed for the purpose of estimating the characteristic strength.

5.4. Variation in shear modulus

The effective shear modulus of elastomeric bearings is obtained from experimental data. LDR and LR bearings show viscoelastic and hysteresis behavior in shear, respectively. The effective stiffness, K_{eff} , is calculated using

$$K_{\text{eff}} = \frac{|F^+| + |F^-|}{|\Delta^+| + |\Delta^-|} \quad (26)$$

where Δ^+ and Δ^- are the maximum and minimum horizontal displacements obtained from an experiment and F^+ and F^- are the corresponding forces. The effective shear modulus is determined using the expression $G_{\text{eff}} = K_{\text{eff}} T_r / A_r$. A typical variation of shear modulus with strain under different nominal axial pressures is shown in Figure 13 for an LDR bearing of 35.5 in. diameter and shape factor 26.

Most of the available mathematical models use a constant shear modulus for elastomeric bearing, although shear modulus varies with strain and axial loads. Increasing the axial pressure reduces the shear modulus. However, if the shear modulus, G , is determined from testing of elastomeric bearings at large strains and under nominal axial pressure, the value of G already includes some effects of axial load. The shear modulus of natural rubber decreases with increasing strain up to 100%, remains relatively constant for shear strain between 100% and 200%, and increases again at shear strains of 200% to 250%. The shear modulus obtained from testing of elastomeric bearings at large strains is used for horizontal stiffness of LDR bearings, post-elastic stiffness of LR bearings, and buckling load calculations.

6. EXPERIMENTAL AND NUMERICAL INVESTIGATION

The above mathematical models of elastomeric bearings were implemented in the software program OpenSees [14] as two new User Elements for LDR and LR bearings. Three sets of experimental data, as shown in Figure 14, were used to investigate the capability of the proposed mathematical model to simulate the behavior of elastomeric bearings under cyclic tensile loading. The cavitation

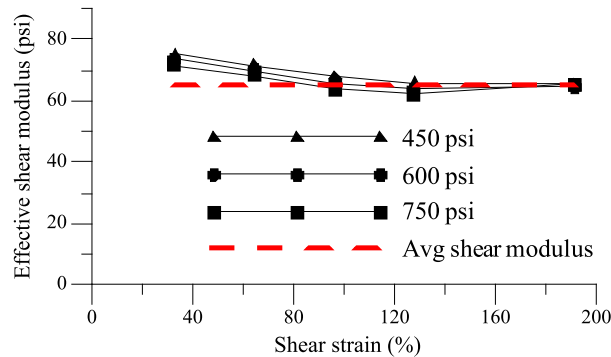


Figure 13. Stress and strain dependence of LDR bearings (courtesy of DIS Inc.).

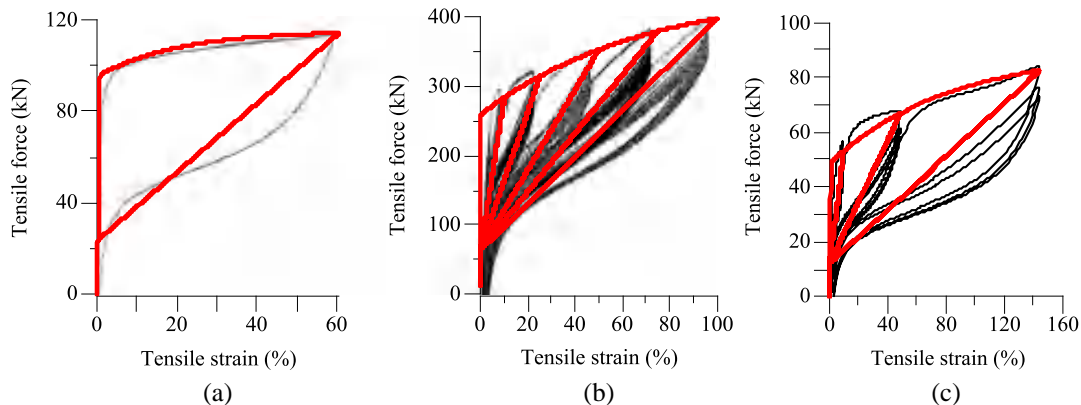


Figure 14. Comparison of experimental and numerical results for LDR bearings in tension. (a) Constantionou *et al.* [1], (b) Iwabe *et al.* [9], and (c) Warn [25].

parameter, k , and the damage index, ϵ_{max} , were obtained by visual calibration of the mathematical model with experimental data. The strength degradation parameter, a , was assumed to be unity. The details of the bearings and the values of parameters estimated by calibration against experimental data are presented in Table III.

The behavior of elastomeric bearings under shear and compression is well established. The strength degradation of LR bearings due to the heating in lead core under cyclic shear loading has already been validated by Kalpakidis *et al.* [41]. However, a comparison of experimental and numerical response using newly created elements is presented in Figure 15 for the same two bearings of [41].

The validation of the mathematical models of coupled horizontal–vertical behavior and varying buckling load capacity of elastomeric bearing is discussed in Warn *et al.* [3].

The effect of cavitation, lateral displacement, and axial force on load–deformation behavior of an elastomeric bearing (LDR 5 in [25]) is shown in Figure 16. The bilinear stiffness model of Constantinou *et al.* [1] ($k = 0$) overestimates the tensile load, and a very small value of the post-cavitation stiffness ($k = 0$) underestimates the tensile load at large tensile displacements. The value of $k=20$ in Figure 16(a) was determined using experimental data of [25]. The maximum damage index, ϵ_{max} , directly affects the energy dissipation capacity and determines the final cavitation strength. The damage index converges to its maximum value following a large tensile deformation after cavitation. Experiments suggest that the value of maximum damage index varies between 0.5 and 0.9 (e.g., [1, 9, 25]). If energy dissipation capacity due to cavitation is to be neglected in the analysis of elastomeric bearings, a very small value of maximum damage index can be used. The vertical stiffness of the bearing decreases with lateral displacement; however, the magnitude still remains very high and should not significantly affect the vertical response of elastomeric bearing. The buckling load capacity of the bearing is affected substantially by the lateral displacement.

The effect of strength degradation parameter on load–deformation behavior in cyclic tension is shown in Figure 17. The strength degradation parameter, a , determines the rate at which the damage index converges to its maximum value, ϵ_{max} , which directly affects the cavitation strength in subsequent cycles under tension. As presented in Figure 14, the value of $a=1.0$ provides a close match with experimental observations.

Table III. Properties of the bearings used for experimental comparison.

	Constantinou <i>et al.</i> [1]	Iwabe <i>et al.</i> [9]	Warn [25]
Diameter (mm)	250	500	164
Shape factor (S)	9.8	33	10.2
Cavitation parameter (λ)	60	15	20
Max. damage index (ϵ_{max})	0.75	0.75	0.75
Strength degrad. parameter (a)	1.0	1.0	1.0

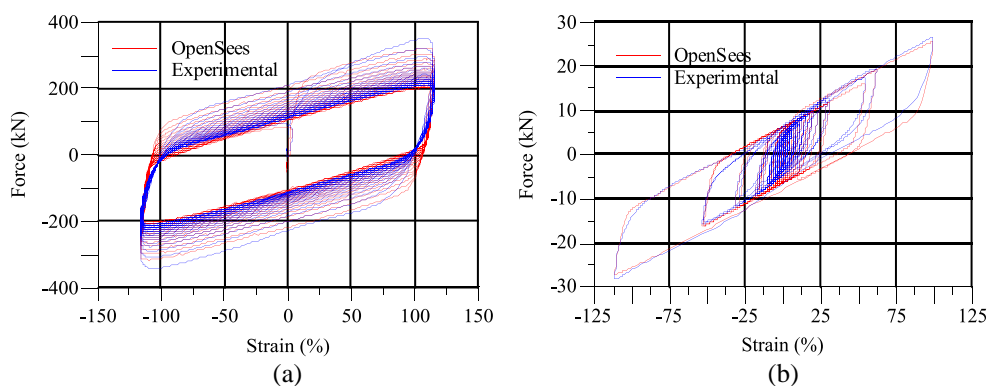


Figure 15. Comparison of experimental and numerical results for LR bearings in shear direction. (a) Large size, harmonic loading, and (b) small size, random loading.

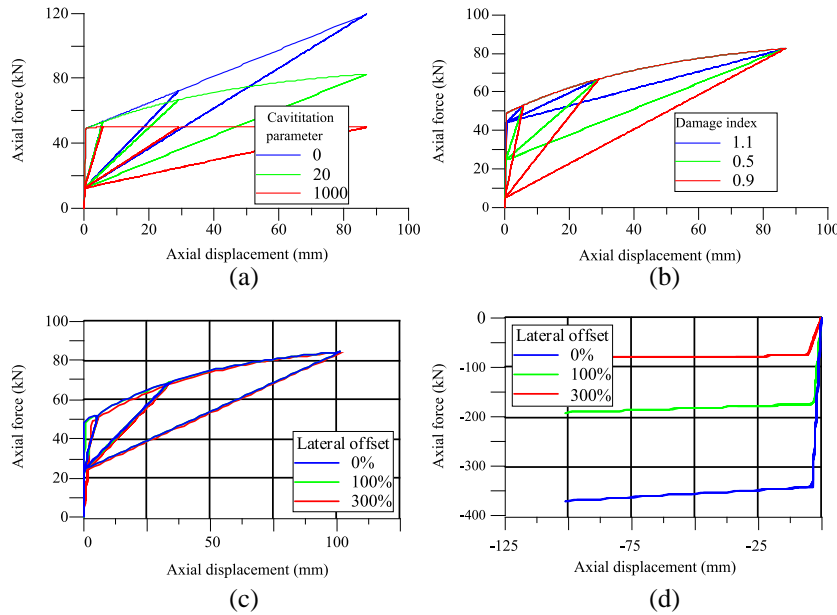


Figure 16. Effect of various parameters on axial load deformation behavior of an LDR bearing. (a) Effect of cavitation parameter, (b) effect of damage index, (c) effect of lateral displacement (tension), and (d) effect of lateral displacement (compression).

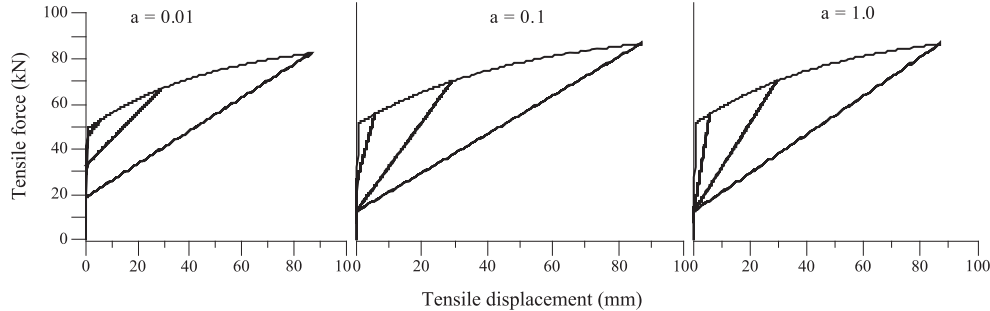


Figure 17. Effect of strength degradation parameter on load deformation behavior in tension.

As discussed previously, the yield strength of an LDR bearing is determined using an assumed value of damping and displacement per Eqn (25). The effect of the damping ratio (ζ_{eff}) and the displacement (D) used in the calculation of yield strength on the shear hysteresis loop of the LDR 5 bearing in Warn [25] is shown in Figure 18.

Warn [25] reported damping ratios of LDR bearings in the range of 2% to 4%. The energy dissipation capacity of an LDR bearing in this damping range, as evident from Figure 18(a), is insignificant and is not expected to significantly affect the shear response of an elastomeric bearing. A small variation in the damping ratio within the range recommended (2% to 4%) for the calculation of yield strength will not significantly affect the shear response of an LDR bearing. The other effect of damping ratio on shear behavior of an LDR bearing is the increase in effective stiffness with damping. However, the effective shear modulus of an LDR bearing calculated from test data already accounts for the effect of damping on shear stiffness. For an assumed value of damping ratio, the energy dissipation capacity of an LDR bearing increases with displacement (D) used in the calculation of the yield strength. However, at a small value of damping ratio, the variations in the displacement, D , do not substantially affect the overall shear response of an LDR bearing, because the shear response of an LDR bearing is dominated by the elastic component of the response with little contribution from the hysteretic component.

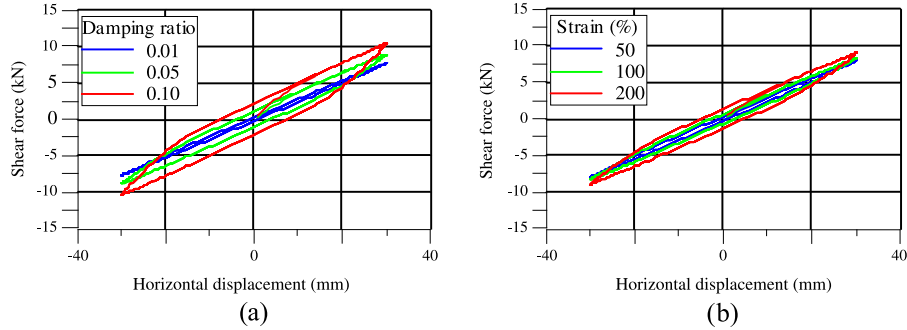


Figure 18. Effect of different parameters on yield strength of an LDR bearing. (a) Varying damping, $D = T_r$ and (b) varying D , damping = 3%.

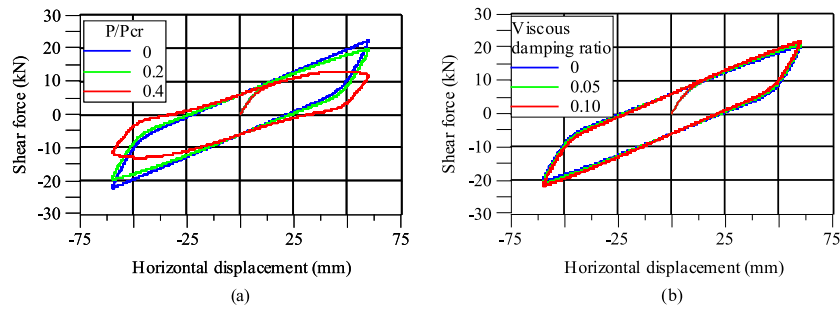


Figure 19. Effect of parameters on the shear behavior of the LR5 bearing of [25]. (a) Axial load and (b) viscous damping.

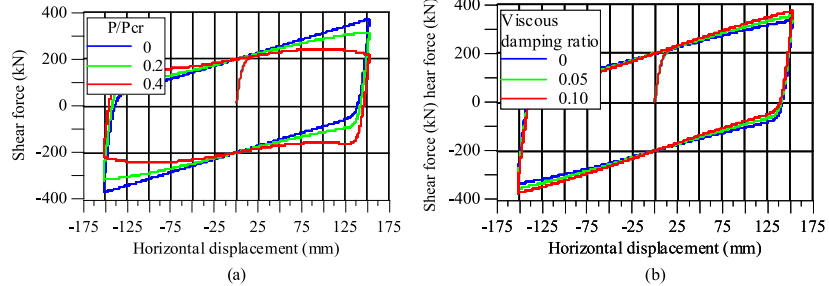


Figure 20. Effect of parameters on the shear behavior of the large size LR bearing of [41]. (a) Axial load and (b) viscous damping.

The effect of axial load on LR5 bearing of [25] and the large size LR bearing in [41] is shown in Figures 19 and 20, respectively. The shear stiffness decreases with axial load, but the effect becomes apparent only when axial load is close to the critical buckling load. The energy dissipation capacity of LR bearing is primarily due to lead, and contribution of viscous damping can be neglected. The effect of viscous damping term ($c_d \dot{U}$) in Eqn (17) on the load-deformation behavior of LR bearing is minor at small displacements.

7. SUMMARY AND CONCLUSIONS

Robust numerical formulations are obtained with the mathematical models of elastomeric bearings. Numerical models are implemented in OpenSees as new user elements, and numerical results

compare well with the experimental data for behavior in tension. In most cases, the strength degradation parameter, a , can be assumed to be unity, and the damage index, δ_{max} , will range between 0.5 and 0.9. The cavitation parameter, k , should be determined experimentally or can be estimated on the basis of the experimental data available for bearings of a similar shape, size, compound, and fabrication. The effect of lateral displacement on vertical stiffness becomes significant only after lateral strain exceeds 100%. The critical buckling load capacity decreases linearly with the overlap area. The very high axial stiffness of an elastomeric bearing, even after significant reduction from the initial value due at large lateral displacements, suggests that the reduction in buckling load capacity, and not the change in vertical stiffness, will be critical under extreme loading.

The viscous damping in an LDR bearing does not provide substantial energy dissipation capacity. An effective damping $\zeta_{eff} = 3\%$ and displacement of $D = T_r$ can be assumed for the calculation of the effective yield strength of an LDR bearing. The yield strength of an LR bearing is determined from the yield stress of the lead core. If test data on viscous damping parameter (c_d) is not available, the damping ratio (and hence c_d) can be assumed to be zero for the analysis of LR bearings. The shear stiffness of an elastomeric bearing decreases when the axial load is close to the critical buckling load of the bearing. A bearing will never realize its axial load capacity (critical buckling load at zero lateral displacement) under three-dimensional excitation as it will fail at an axial load lower than the critical load because of the nonzero lateral displacement. The use of a constant value for the critical buckling load, calculated at zero lateral displacement, might compromise the performance of an isolator and the isolation system.

ACKNOWLEDGEMENTS

This research project is supported by a grant to MCEER from the United States Nuclear Regulatory Commission (USNRC) and the Lawrence Berkeley National Laboratory (LBNL). This financial support is gratefully acknowledged. The authors thank Dr Annie Kammerer of USNRC and Dr Robert Budnitz of LBNL, and former University at Buffalo graduate students Dr Ioannis Kalpakidis of Energo Engineering and Dr Gordon Warn of Penn State University for providing test data on elastomeric bearings.

REFERENCES

- Constantinou MC, Whittaker AS, Kalpakidis Y, Fenz DM, Warn GP. *Performance of Seismic Isolation Hardware Under Service and Seismic Loading*. MCEER-07-0012, Multidisciplinary Center for Earthquake Engineering Research, University at Buffalo: New York, 2007.
- Koh CG, Kelly JM. *Effects of Axial Load on Elastomeric Isolation Bearings*. EERC/UBC 86/12, Earthquake Engineering Research Center, University of California: Berkeley, United States, 1987; 108.
- Warn GP, Whittaker AS, Constantinou MC. Vertical stiffness of elastomeric and lead-rubber seismic isolation bearings. *Journal of Structural Engineering* 2007; 133(9):1227–1236.
- Yamamoto S, Kikuchi M, Ueda M, Aiken ID. A mechanical model for elastomeric seismic isolation bearings including the influence of axial load. *Earthquake Engineering and Structural Dynamics* 2009; 38(2):157–180.
- Gent AN, Lindley PB. The compression of bonded rubber blocks. *Proceedings of the Institution of Mechanical Engineers* 1959; 173(1):111–122.
- Dorfmann A, Burtscher SL. Aspects of cavitation damage in seismic bearings. *Journal of Structural Engineering* 2000; 126(5):573–579.
- Dorfmann A, Fuller KNG, Ogden RW. Shear, compressive and dilatational response of rubberlike solids subject to cavitation damage. *International Journal of Solids and Structures* 2002; 39:1845–1861.
- Yang QR, Liu WG, He WF, Feng DM. Tensile stiffness and deformation model of rubber isolators in tension and tension-shear states. *Journal of Engineering Mechanics* 2010; 136(4):429–437.
- Iwabe N, Takayama M, Kani N, Wada A. Experimental study on the effect of tension for rubber bearings. *Proceedings of the 12th World Conference on Earthquake Engineering*, New Zealand, 2000.
- Kikuchi M, Nakamura T, Aiken ID. Three-dimensional analysis for square seismic isolation bearings under large shear deformations and high axial loads. *Earthquake Engineering and Structural Dynamics* 2010; 39(13):1513–1531.
- United States Nuclear Regulatory Commission (USNRC). *Technical Considerations for Seismic Isolation of Nuclear Facilities*. NUREG-xxxx: Washington DC, forthcoming.
- American Society of Civil Engineers (ASCE). *Seismic Analysis of Safety-Related Nuclear Structures and Commentary ASCE 4-13*, American Society of Civil Engineers (ASCE): Reston, VA, forthcoming.
- The American Society of Mechanical Engineers (ASME). *Guide for Verification and Validation in Computational Solid Mechanics. ASME V&V 10-2006*, American Society of Mechanical Engineers (ASME): New York, NY, 2006.
- McKenna F, Fenves G, Scott M. Computer program OpenSees: open system for earthquake engineering simulation, Pacific Earthquake Engineering Center, University of California, Berkeley, CA, 2006. (Available from: <http://opensees.berkeley.edu>) [Accessed on August 2013].

15. Ryan KL, Kelly JM, Chopra AK. Nonlinear model for lead-rubber bearings including axial-load effects. *Journal of Engineering Mechanics* 2005; 131(12):1270–1278.
16. Vu B, Unal M, Warn GP, Memari AM. A distributed flexibility and damping strategy to control vertical accelerations in base-isolated buildings. *Structural Control and Health Monitoring* 2013; DOI: 10.1002/stc.1580.
17. Japan Road Association (JRA). *Bearing Support Design Guide for Highway Bridges (in Japanese)*. Japan Road Association (JRA): Japan, 2012.
18. European Committee for Standardisation (ECS). *Eurocode 8: Design of Structures for Earthquake Resistance—Part 2: Bridges*. EN 1998-2, European Committee for Standardisation (ECS): Brussels, Belgium, 2005.
19. Ministry of Construction of the People's Republic of China, China Architecture & Building Press (MOPRC). *Code for Seismic Design of Buildings (in Chinese)*. GB50011-2010, China Architecture & Building Press: Beijing, China, 2010.
20. Gent AN, Lindley PB. Internal rupture of bonded rubber cylinders in tension. *Royal Society of London* 1959; 249(1257):195–205.
21. Clark PW. Experimental studies of the ultimate behavior of seismically-isolated structures. Ph.D. Dissertation, University of California at Berkeley, CA, 1996.
22. Takayama M, Oka K, Kato R. The tensile tests of natural rubber bearing focused on the effect of the steel flange plates. *13th World Conference on Earthquake Engineering*, Vancouver, Canada, 2004.
23. Shoji G, Saito K, Kameda T, Fueki T. Seismic performance of a laminated rubber bearing under tensile axial loading. *13th World Conference on Earthquake Engineering*, August 1–6, 2004, Vancouver, Canada, 2004.
24. Feng D, Miyama T, Lu X, Ikenaga M. A shaking table test study on shear tensile properties of lead rubber bearings. *13th World Conference on Earthquake Engineering*, August 1–6, 2004, Vancouver, Canada, 2004.
25. Warn GP. The coupled horizontal–vertical response of elastomeric and lead-rubber seismic isolation bearings. PhD Dissertation, Civil, Structural and Environmental Engineering, University at Buffalo, 2006.
26. Gent A. Cavitation in rubber: a cautionary tale. *Rubber Chemistry and Technology* 1990; 63:49.
27. Gent AN. *Engineering with Rubber: How to Design Rubber Components*. Hanser Gardner Publications: Munich, 2001; 365.
28. Stanton JF, Roeder CW. Elastomeric bearings design, construction, and materials: NCHRP Report 248. 0077-5614, Transportation Research Boards, Washington, DC, 1982.
29. Kelly JM. *Earthquake-Resistant Design with Rubber*. Springer-Verlag: London, 1993.
30. Haringx JA. On highly compressible helical springs and rubber rods, and their application for vibration-free mountings—part 1, 2, 3. Philips Research Reports, 1948.
31. Han X, Kelleher C, Warn G, Wagener T. Identification of the controlling mechanism for predicting critical loads in elastomeric bearings. *Journal of Structural Engineering* 2013; 139(12).
32. Buckle IG, Liu H. Stability of elastomeric seismic isolation systems. *Proceedings of the Seminar on Seismic Isolation, Passive Energy Dissipation, and Control*, Redwood City, California, 1993; 293–305.
33. Weisman J, Warn GP. Stability of elastomeric and lead-rubber seismic isolation bearings. *Journal of Structural Engineering* 2012; 138(2):215–223.
34. Sanchez J, Masroor A, Mosqueda G, Ryan K. Static and dynamic stability of elastomeric bearings for seismic protection of structures. *Journal of Structural Engineering* 2013; 139(7):1149–1159.
35. Wen Y-K. Method for random vibration of hysteretic systems. *Journal of the Engineering Mechanics Division* 1976; 102(2):249–263.
36. Park YJ, Wen YK, Ang AHS. Random vibration of hysteretic systems under bi-directional ground motions. *Earthquake Engineering and Structural Dynamics* 1986; 14(4):543–557.
37. Nagarajaiah S, Reinhorn AM, Constantinou MC. *Nonlinear Dynamic Analysis of Three-Dimensional Base Isolated Structures (3D-BASIS)*. NCEER-89-0019, National Center for Earthquake Engineering Research, University at Buffalo: United States, 1989; 132.
38. Mokha AS, Constantinou MC, Reinhorn AM. Verification of friction model of teflon bearings under triaxial load. *Journal of Structural Engineering New York, N.Y.* 1993; 119(1):240–261.
39. Nagarajaiah S, Reinhorn AM, Constantinou MC. Nonlinear dynamic analysis of 3-d-base-isolated structures. *Journal of Structural Engineering New York, N.Y.* 1991; 117(7):2035–2054.
40. Constantinou MC, Adnane MA. *Dynamics of Soil-Base-Isolated-Structure Systems: Evaluation of Two Models for Yielding Systems*, No. 4 to NSF, Drexel University: Philadelphia, 1987.
41. Kalpakidis IV, Constantinou MC, Whittaker AS. Modeling strength degradation in lead-rubber bearings under earthquake shaking. *Earthquake Engineering and Structural Dynamics* 2010; 39(13):1533–1549.
42. American Association of State Highway and Transportation Officials (AASHTO). *Guide Specifications for Seismic Isolation Design*. American Association of State Highway and Transportation Officials (AASHTO): Washington, D.C., 2010.
43. American Society of Civil Engineers (ASCE). *Minimum Design Loads for Buildings and Other Structures*. ASCE 7-10, American Society of Civil Engineers (ASCE): Reston, VA, 2010.
44. Constantinou M, Kalpakidis I, Filiatru A, Lay RAE. *LRFD-Based Analysis and Design Procedures for Bridge Bearings and Seismic Isolators*. MCEER-11-0004, Multidisciplinary Center for Earthquake Engineering Research, University at Buffalo: NY, 2011.